ELSEVIER

International Journal of Adhesion & Adhesives 29 (2009) 45–55

International Journal of Adhesion & Adhesives

www.elsevier.com/locate/ijadhadh

Crack-growth behavior of epoxy adhesives modified with liquid rubber and cross-linked rubber particles under mode I loading

Makoto Imanaka[a,*], Satoshi Motohashi[a], Kazuaki Nishi[a], Yoshinobu Nakamura[b], Masaki Kimoto[c]

[a]*Department of Technology Education, Osaka University of Education, Kashiwara, Osaka 582-8582, Japan*
[b]*Department of Applied Chemistry, Osaka Institute of Technology, Asahi, Osaka 535-8582, Japan*
[c]*Division of Material Technology, Technical Research Institute of Osaka Prefecture, Izumi, Osaka 594-1157, Japan*

Accepted 5 November 2007
Available online 4 February 2008

Abstract

The crack-growth resistance (*R*-curve) of bulk single-edge notch bend (SENB) and adhesively bonded double cantilever beam (DCB) specimens was investigated under mode I loading conditions using two types of rubber-modified epoxy adhesive: one was a liquid rubber (CTBN)-modified adhesive and the other was a cross-linked rubber particle (DCS)-modified adhesive. As a result, for both the SENB and DCB specimens, the gradient of the *R*-curve for the DCS-modified adhesive was steeper than that for the CTBN-modified one, however, the difference in fracture toughness between DCS- and CTBN-modified adhesives is smaller for DCB than for SENB specimens. To elucidate such behavior, crack-growth simulation based on Gurson's model was conducted, where the DCS- and CTBN-modified adhesives were characterized by both the initial void fraction and nucleation. The difference in the behavior of *R*-curves was also observed in simulations. Moreover, it was found that the difference in fracture surface roughness observed by SEM for both adhesives correspond to the variation in *R*-curves.

Keywords: A. Epoxy; M. Fracture mechanics; M. Double cantilever beam specimen

1. Introduction

Rubber-modified epoxy adhesives have attracted special interest due to their property of satisfying static strength and toughness simultaneously. Numerous studies have been conducted on the fracture toughness of several types of adhesive joints bonded by rubber-modified adhesives [1–3].

There are two types of rubber-modified epoxy resin. One is a liquid rubber-modified epoxy resin. The rubber particles are precipitated by phase separation from the homogeneous phase, and are well dispersed in the resin. The other type has cross-linked or core–shell rubber particles in the epoxy resin. As the rubber particles are mixed with epoxy resin, aggregation of the particles occurs, and the dispersion state is inferior to that of the precipitation type. Recently, it was reported that the toughening mechanisms for liquid rubber-modified epoxies differ from those for core–shell rubber particle-modified ones [4–8]. Some papers have reported that the fracture toughness of core–shell rubber particle-modified epoxies is higher than that of liquid rubber-modified ones [7,8]. However, there have been few studies on the fracture toughness of adhesively bonded joints with cross-linked rubber particle or core–shell rubber particle-modified epoxy resins [9].

Fracture toughness of ductile materials is, in general, characterized by the crack-growth resistance (*R*-curve). In most studies on rubber-modified epoxies, however, crack propagation occurs when the energy release rate reaches a critical value. There are few studies on *R*-curve behavior in rubber-modified epoxy resins. Most recently, the *R*-curve behavior of liquid rubber-modified epoxy resin has been studied using bulk double cantilever beam (DCB) specimens [10] and adhesively bonded DCB specimens [11,12].

*Corresponding author. Tel./fax: +81 72 978 3444.
E-mail address: imanaka@cc.osaka-kyoiku.ac.jp (M. Imanaka).

0143-7496/$ - see front matter © 2008 Elsevier Ltd. All rights reserved.
doi:10.1016/j.ijadhadh.2007.11.004

Thus, it is important to investigate the *R*-curve behavior of the adhesive joints modified with cross-linked rubber particles or core–shell rubber. This will facilitate further improvement of the fracture toughness of rubber-modified adhesives.

In this study, the *R*-curve behavior of two kinds of rubber-modified epoxy adhesives was investigated using adhesively bonded DCB specimens under mode I loading conditions, in order to clarify the difference in *R*-curve behavior between liquid rubber-modified and cross-linked rubber particle-modified epoxy adhesives. Furthermore, single-edge notch bend (SENB) tests were conducted to compare the *R*-curve behavior of the DCB specimens with that of the bulk adhesive ones. To elucidate the difference, crack-growth simulation based on Gurson's model and SEM observations of the fractured surfaces were also conducted.

2. Experimental procedure

2.1. Adhesives

The compositions of the two types of adhesives used in this study are given in Table 1. One is a cross-linked rubber particle (DCS)-dispersed system, and the other is a carboxy-terminated butadiene-acrylonitrile (CTBN)-modified one. Reactive diluent (YED111) was used to improve the deformability of the matrix phase for both adhesives: the contents of YED111 and rubber particles are 20 and 13 phr, respectively. The diameters of the rubber particles for CTBN- and DCS-modified adhesives are in the ranges of about 3–6 μm and 300–700 nm, respectively; thus, CTBN rubber particles were about 10 times as large as those of the DCS.

Dumbbell specimens (JIS.K7113) were used to measure the stress–strain curves under tensile loading for the two bulk adhesives and matrix resins. Fig. 1 shows the stress–strain curves under tensile loading for the two adhesives and the matrix resins with and without YED111, wherein engineering strain was measured by a clip gage and the engineering stress was given as the ordinate. In this figure, the matrix without YED111 exhibits a brittle behavior, whereas the one with YED111 shows a ductile behavior, and the elongation markedly improved. This figure also indicates that the initial slopes and peak stresses for both DCS- and CTBN-modified adhesives are nearly equal to those for the matrix resin with YED111, which reveals that the elastic modulus and peak stresses do not deteriorate through the rubber modifications. Also, Young's modulus was determined from the gradient of stress–strain curve in the elastic range, and Poisson's ratio of the bulk specimens was determined from the strains in the longitudinal and lateral directions, which were measured by a two-directional strain gage pasted on the dumbbell specimen. The obtained elastic constants of the matrix resin for the adhesives are listed in Table 2, including the yield stress and work-hardening parameters.

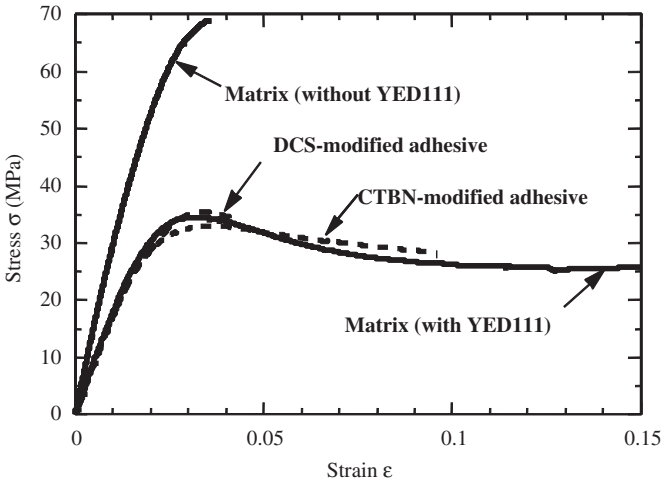

Fig. 1. Stress–strain curves of the matrix resins.

Table 2
Material constants of the adherend and matrix of the adhesive

Adherend	Young's modulus: 205.8 GPa Poisson's ratio: 0.33	
Matrix resin of the adhesive	Young's modulus: 1793 MPa Poisson's ratio: 0.38 Yield stress: 23.6 MPa	
	Work hardening data	
	Plastic strain, ε_p	Stress (MPa)
	2.1×10^{-3}	28.9
	4.2×10^{-3}	32.3
	8.5×10^{-3}	33.6
	1.14×10^{-2}	34.3

Table 1
Formations of epoxy adhesives

Rubber type	DGEBA epoxy resin (g)	Reactive diluent (g)	Rubber (g)	Curing agent (g)
DCS-1	100	20	15.6	6
CTBN 1300 × 8	100	20	15.6	6

Epoxy resin: Epikote 828 Japan Epoxy Resin Co. Ltd.; reactive diluent: YED111 Japan Epoxy Resin Co. Ltd.; DCS-1 cross-linked rubber particles (JSR); CTBN 1300 × 8 (Ube Industries Ltd.); curing agent: piperidine.

2.2. Single-edge notch bend tests for the bulk adhesives

The J–R-curve of the bulk adhesive specimens was measured by a three-point bending test as illustrated in Fig. 2. The cross-head speeds of loading and unloading cycles were 0.5 and 50 mm/min, respectively. To introduce a pre-crack, a sharp incision was made on the base of the slot of the SENB specimen, maintained at 373 K using a fresh razor blade (Microtome knives, T-40, Nippon Microtome Laboratory Co. Ltd., Japan), where the pre-crack length ranged from about 4.5 to 5.5 mm. After unloading, the specimen was cooled in liquid nitrogen and then broken immediately for measuring the crack extension.

The J integral value was calculated from Eq. (1) as the integral intensity of the load–displacement curve based on the method according to ASTM-E-1820-99A:

$$J = \frac{K^2(1-\nu^2)}{E} + \frac{2U_p}{B(W-a_0)}, \quad (1)$$

where K is the stress intensity factor, E the Young's modulus, ν the Poisson's ratio, W and B the width and thickness of the specimen, respectively, a_0 the pre-crack length, and U_p the plastic work. A detailed calculation method is available elsewhere [13].

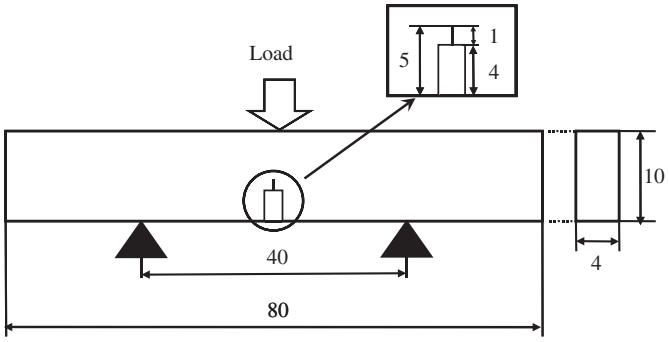

Fig. 2. Shape and sizes of SENB specimen.

2.3. Adhesively bonded double cantilever beam specimens

Fig. 3 shows the shape and size of the DCB specimen used in this work. Structural carbon steel JIS S55C was used as the adherend. Applied loads were transmitted to the DCB specimen via loading pins. Hence, loading points could be rotated. A filler gauge of 0.01 mm in thickness, treated by a release agent, was adopted as a pre-crack with the adhesive layer thickness being adjusted to 0.4 mm. The cross-head speeds of loading and unloading cycles were 5 and 50 mm/min, respectively. To measure crack extension, a crack tip was immersed in a solution of fluorescent agent during the loading test. After unloading the specimen was broken at a cross-head speed of 500 mm/min, the crack extension being measured from the fracture surface using a measuring microscope under UV light.

The energy release rate, G, was evaluated from Eq. (2):

$$G = \frac{P^2}{2B}\frac{dC}{da}, \quad (2)$$

where P is the applied load, and the compliance, C was experimentally measured with various crack lengths, a. dC/da was obtained from the regression equation between the cube root of the compliance and crack length.

3. Experimental results

3.1. Load–displacement curves

Fig. 4(a) and (b) shows typical examples of the load–displacement curves for SENB and DCB specimens. The crack extensions just before unloading, Δa, and the initial crack length, a_0, are also indicated in the figure. The initial slopes of the load–displacement curves for SENB specimens are different in each case, as in Fig. 4(a), which is due to the difference in the initial crack length. The maximum value of the load–displacement curve for SENB specimens with the DCS-modified adhesive is about 1.3–2 times greater than that of the CTBN-modified adhesive. For the DCB specimens, the maximum value

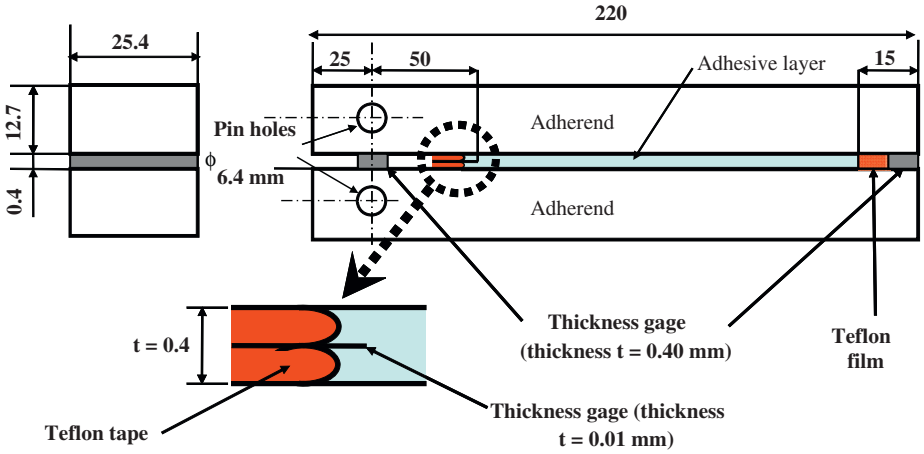

Fig. 3. Shape and sizes of the adhesively bonded DCB specimen.

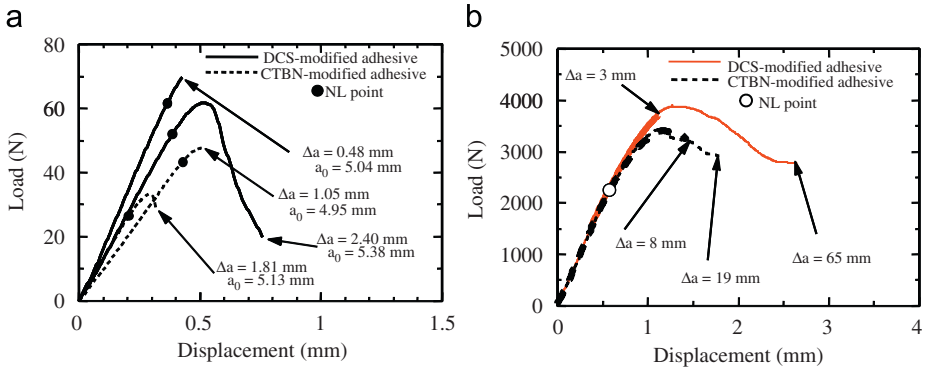

Fig. 4. Load–displacement curves for (a) SENB and (b) DCB specimens.

of the DCS-modified adhesive is also greater than that of the CTBN-modified one. However, the difference between DCS- and CTBN-modified adhesives is small compared to that of the SENB specimen as shown in Fig. 4(b).

Here, the points which deviate from linearity are indicated as non-linear (NL) points. In general, crack propagation in adhesives begins at such points. For SENB specimens, the differences between NL and peak points as well as the crack extensions near the peak points are small. This agrees with the general trend mentioned above. In contrast, for the DCB specimen, the difference in the load between NL and peak points is greater than that for SENB specimens, where the load at the NL point is about 60–70% of the peak value; however, crack extension at the peak points is small. Thus, it is expected that the damage zone is generated prior to crack propagation, which will be discussed later in the analytical section.

3.2. *R*-curves

The *R*-curves of the SENB specimens with DCS- and CTBN-modified adhesives are shown in Fig. 5. As shown in this figure, J for DCS-modified adhesive is higher than those for CTBN-modified adhesive, irrespective of the crack growth, and the difference in J between CTBN- and DCS-modified adhesives increases with crack growth. This figure also shows that J for the CTBN-modified adhesive is independent of crack growth, which indicates that no *R*-curve behavior appears for the bulk CTBN adhesive. In contrast, for the DCS-modified adhesive, although the plots with Δa smaller than 0.1 mm are scattered, a gentle rise of J is found with Δa smaller than 1 mm, and there is a sharp elevation in J with further growth to about 2 mm. High J values distribute around $\Delta a = 2$ mm, where the ratio of the total crack length to the width of the specimen (a/W) lies between 0.7 and 0.8. In such a short ligament range, the *R*-curve may rise, even though the intrinsic crack propagation resistance does not change [14]. Thus, the intrinsic crack-growth resistance for DCS-modified adhesive is considered to be a little larger than that for CTBN-modified adhesive.

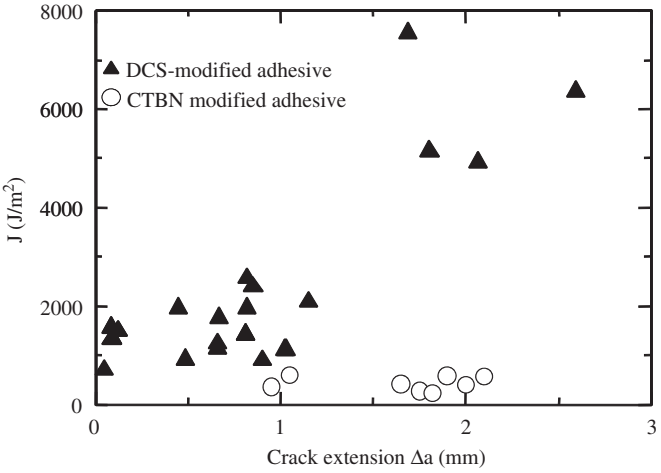

Fig. 5. *R*-curves for SENB specimens.

Fig. 6 shows the *R*-curves of the DCB specimens with DCS- and CTBN-modified adhesives. The value of the critical energy release rate, G_{1C}, for the DCS-modified adhesive shows a peak value at $\Delta a = 30$ mm and then slows down to a steady-state value of $\sim 4\,kJ/m^2$. For the CTBN-modified adhesive, most data points for G_{1C} fall on a line with a less pronounced slope than the plots of DCS-modified adhesive at $\Delta a < 20$ mm, though the plots below 5 mm are scattered. Then, G_{1C} gradually rises to a plateau value of $\sim 4\,kJ/m^2$. Initial toughness values of the adhesive in the joints are, in general, lower than their bulk ones. As Figs. 5 and 6 show, the relation of the initial toughness values between adhesively bonded joints and bulk specimens is, however, reverse to the usual one. In this work, J integral values were measured in the range of $\Delta a < 2$ mm for the bulk SEBN specimens, whereas critical energy release rates were done in the range of $2\,mm < \Delta a < 90$ mm for the adhesively bonded DCB specimens. Crack growth was measured from the fracture surface after the unloading cycle. Thus, it was difficult to determine the energy release rate, G_{1C}, in the short crack-growth range corresponding to the bulk specimens. The value for G_{1C} at $\Delta a < 2$ mm is unclear, but there is a possibility that it suddenly drops in the range.

It is also observed from Figs. 5 and 6 that the difference in *R*-curves between CTBN- and DCS-modified adhesives for the bulk specimens is greater than that for the adhesively bonded DCB specimens. Recently, Yan et al. [8] have compared the fracture toughness of CTBN-modified epoxy resin with that of a core–shell rubber-modified one, using compact tension (CT) and DCB laminate specimens under mode I loading. They found that the fracture toughness of the bulk CT specimen with the core–shell rubber-modified resin is higher than that with the CTBN-modified one. Contrary to the bulk specimen, the fracture toughness of the DCB specimen modified with the core–shell rubber is lower than that with the CTBN-modified one. They suggested that high constraint conditions reduced the fracture toughness of core–shell rubber-modified epoxy. Such a trend is similar to the difference in *R*-curve characteristics between SENB and DCB specimens. The reason for the difference will be discussed later from another point of view.

3.3. Fracture surface observations

Fig. 7(a) and (b) shows SEM images of the fracture surfaces for the SENB specimens with CTBN- and DCS-modified adhesives. As Fig. 7(a) shows, the rubber particles in CTBN-modified adhesive are well dispersed, and the fracture surface is flat; moreover, plastic deformation lines are scarcely observed, which indicates that the matrix shear yielding does not fully extend. This may be one reason for the low fracture toughness of the CTBN-modified adhesive. In Fig. 7(b), on the other hand, the fracture surfaces of the DCS-modified adhesive shows that the trace of cavities is localized owing to the lower dispersability of DCS particle than that of CTBN ones. The matrix of DCS-modified adhesive is, however, deformed more severely than that of the CTBN one. In general, a rough surface improves the fracture toughness. Thus, it is expected that the rough surface of DCS-modified adhesive is one of the reasons for its high toughness.

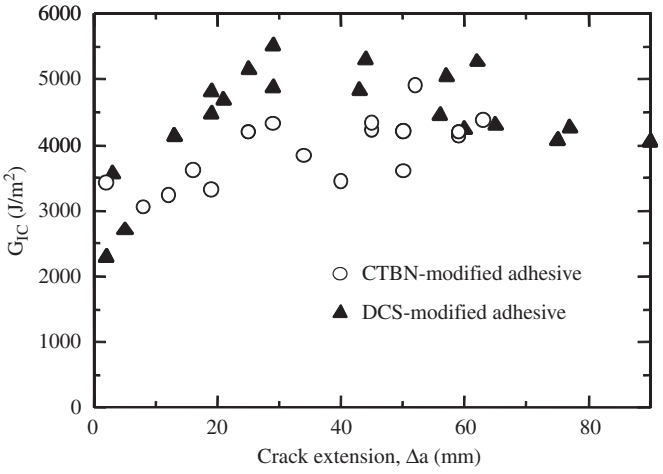

Fig. 6. *R*-curves for DCB specimens.

Fig. 8 shows a macroscopic view of fracture surfaces of the DCB specimens. From the figure, a cohesive fracture pattern is observed in the DCS-modified adhesive, whereas serrated interfacial failure is noted in the CTBN-modified adhesive. This means that the crack is apt to propagate near the interface for the CTBN-modified adhesive. Daghyani et al. showed that *T*-stress induced from residual stress affects the fracture locus, and that the crack locus varies with the sign of the *T*-stress value [15]. As the pre-crack was induced in the middle of the adhesive layer, the crack trajectory is dependent on the sign of the *T*-stress: negative *T*-stress leads to crack propagation along the center line of the adhesive layer, and a positive *T*-stress brings wavy crack propagation. Wavy cracks did not appear in either the CTBN- or DCS-modified adhesive. Hence, the residual stress is not considered to be the main reason to explain the difference in the fracture pattern between CTBN- and DCS-modified adhesives. The reason should be searched elsewhere.

Lee et al. indicated that the mean size of dispersed rubber particles near the interface was greater than that in the middle of the adhesive layer, where they used adhesively bonded CT specimens with a CTBN-modified adhesive. Furthermore, the damage zone formed not only ahead of the crack tip but also in the vicinity of the interface [16]. They suggested that the branching of a damage zone ahead of the pre-crack tip into the upper and lower interface damage zones increases the fracture toughness. Evolution of the interfacial damage zone may

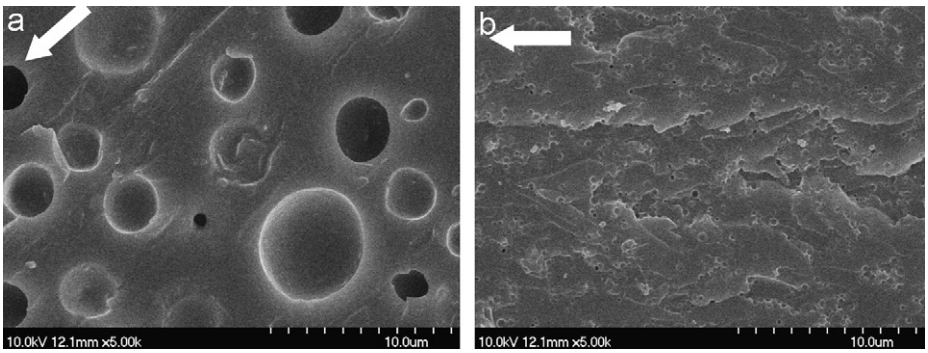

Fig. 7. SEM images of the fracture surfaces for SENB specimens: (a) CTBN-modified adhesive and (b) DCS-modified adhesive.

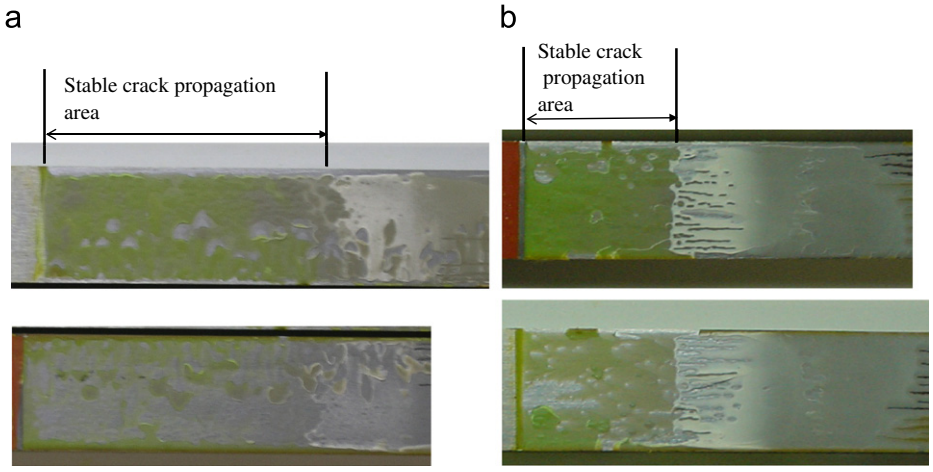

Fig. 8. Macroscopic view of the fracture surfaces for DCB specimens: (a) CTBN-modified adhesive and (b) DCS-modified adhesive.

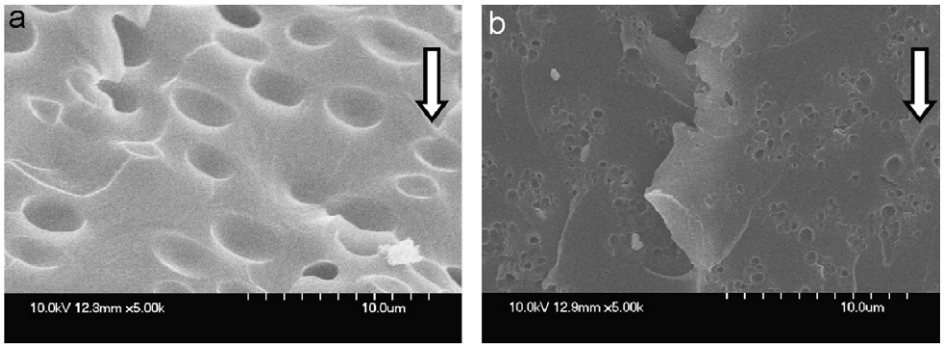

Fig. 9. SEM images of the fracture surfaces for DCB specimens: (a) CTBN-modified adhesive and (b) DCS-modified adhesive.

facilitate serrated interfacial failure, as in Fig. 8. Such explanations for the CTBN-modified adhesive support the occurrence of serrated interfacial failure and high fracture toughness compared with the bulk specimen.

SEM images of the fracture surfaces are shown in Fig. 9. The fracture surface of CTBN-modified adhesive is similar to that of the SENB specimen, where swelling of the DCB specimen is slightly greater than that of the SENB specimen. For the DCS-modified adhesive, the void volume fraction of the DCB specimen is lower than that of the SENB specimen, and its roughness is smaller than that of the SENB specimen, as in Figs. 7(b) and 9(b). This indicates that the matrix of the DCB specimen is less deformed than that of the SENB one, and also leads to the difference whereby the fracture toughness between CTBN- and DCS-modified adhesives for the DCB specimens is smaller than that for the SENB specimens, as in Figs. 5 and 6. Yan et al. also reported the following observations on the fracture surfaces in core–shell rubber-modified epoxies: for the bulk specimen with core–shell rubber-modified epoxy plastic yielding was found, but shear yielding was rarely observed for DCB composite specimens. This implies that shear yielding was suppressed by the constraint [8]. Such a trend is similar to the differences between SENB and DCB specimens of DCS-modified adhesives.

4. Simulation of crack growth based on Gurson's model

It has been well established for many kinds of rubber-modified adhesives that cavitation from rubber particles or debonding occurs near the crack tip due to high stress triaxiality; thus, it can be considered that rubber-modified adhesives behave essentially as porous materials. Gurson's model modified by Tvergaard and Needeleman (GNT model) is widely applicable for estimating the yield and crack propagation behavior of ductile materials [9,17,18]. Recently, this model was applied to estimate the yield stress and fracture toughness for rubber-modified epoxy resins and adhesives [19,20].

The yield criterion for the macroscopic assembly of voids and matrix material is given by

$$F = \left(\frac{\sigma_{\mathrm{M}}}{\sigma_{\mathrm{y}}}\right)^2 + 2q_1 f \cosh\left(\frac{q_2\sigma_{kk}}{2\sigma_{\mathrm{y}}}\right) - \{1 - (q_1 f)^2\} = 0, \quad (3)$$

where F is the yield function, σ_{y} the yield stress of the matrix, σ_{kk} the first stress invariant, f the void volume fraction, σ_{M} the Mises equivalent stress, and q_1 and q_2 the parameters.

In the present analysis, as the coalescence of voids was not considered, so that the existing value of the void

volume fraction varied with the growth of existing voids and the nucleation of new voids, then its rate could be expressed as

$$\dot{f} = \dot{f}_{\text{growth}} + \dot{f}_{\text{nucleation}}. \tag{4}$$

The growth rate of voids can be determined based on the compressibility of the matrix material as follows:

$$\dot{f}_{\text{growth}} = (1-f)\dot{\varepsilon}^{\text{p}}_{kk}, \tag{5}$$

where $\dot{\varepsilon}^{\text{p}}_{kk}$ is the hydrostatic strain of the plastic.

The nucleation rate, $\dot{f}_{\text{nucleation}}$ controlled by the mean stress, is given as follows:

$$\dot{f}_{\text{nucleation}} = \frac{f_{\text{N}}}{S\sqrt{2\pi}} \exp\left[-\frac{1}{2}\left(\frac{\sigma_{kk}/3 - \sigma_{\text{m}}}{S}\right)^2\right]\frac{\dot{\sigma}_{kk}}{3}, \tag{6}$$

where f_{N} is the volume fraction of void forming particles, S the standard deviation, $\sigma_{kk}/3$ the mean stress, and σ_{m} the mean stress for void nucleation.

Fig. 10 shows the boundary conditions and mesh pattern near the crack tip for DCB and SENB specimens. For both specimens, only half of the specimen was modeled because of their symmetrical-ness. Large deformation plane strain finite element analysis was carried out with the finite element code MSC-Marc, wherein the above Gurson's yield criterion and algorithm of the damage evolution are incorporated. The simulation methodology for crack propagation is as follows: When the void volume fraction, f, in the element incident to the current crack tip reaches a critical value, f_{E}, the elements lose their stress-carrying capability. Hereafter, this element was treated as a crack. For the two joints, the mesh size was unified to $D = 0.03$ mm in the hatched zone in Fig. 10.

In the application of the GNT model to the adhesive layer, Gurson's parameters are required for the CTBN- and DCS- modified adhesives. To determine these parameters, the following assumptions are adopted: For CTBN-modified adhesive, rubber particles are treated as the initial voids, because the particles easily expand; thus, nucleation disregarded. This assumption does not conflict with the SEM observation, as in Fig. 9, because the void fraction was high enough to assume that the rubber particles were initial voids. On the other hand, the above assumption cannot apply to the DCS-modified adhesive, because the void fraction observed in the fracture surface is too small to assume that the rubber particles existed as initial voids. Furthermore, rubber particles in DCS-modified adhesive are rigid, and so cannot easily expand. Hence, it is assumed that debonding, i.e., nucleation, occurs when the dilational stress reaches a critical stress. Both the elastic and plastic constants of the matrix resin are assumed to be the same as for the adhesives, which are listed in Table 2, as above mentioned. The initial void fraction of CTBN-modified adhesive was assumed to be 0.14 from the weight fraction of the rubber content, because the rubber particles are treated as initial voids. Due to the nucleation, the initial void fraction, f_{i}, of DCS-modified adhesive was assumed to be less than that of CTBN-modified adhesive. From the observation of the fracture surface, the void fraction of DCS-modified adhesive is less than that of the CTBN-modified one. Hence, the critical void volume fraction of CTBN-modified adhesive at failure, f_{E}, was assumed to be greater than that of DCS-modified adhesive. In Eq. (3), Gurson's parameter q_2 is generally assumed to be 1.0. A numerical study showed that the value of $q_1 = 1.5$ is applicable for solids with periodically spaced voids at a low void fraction [21]. However, this value cannot be used for the rubber-modified adhesives due to the high void fraction. In the present situation, theoretical analysis of q_1 was not conducted for solids with a high void fraction.

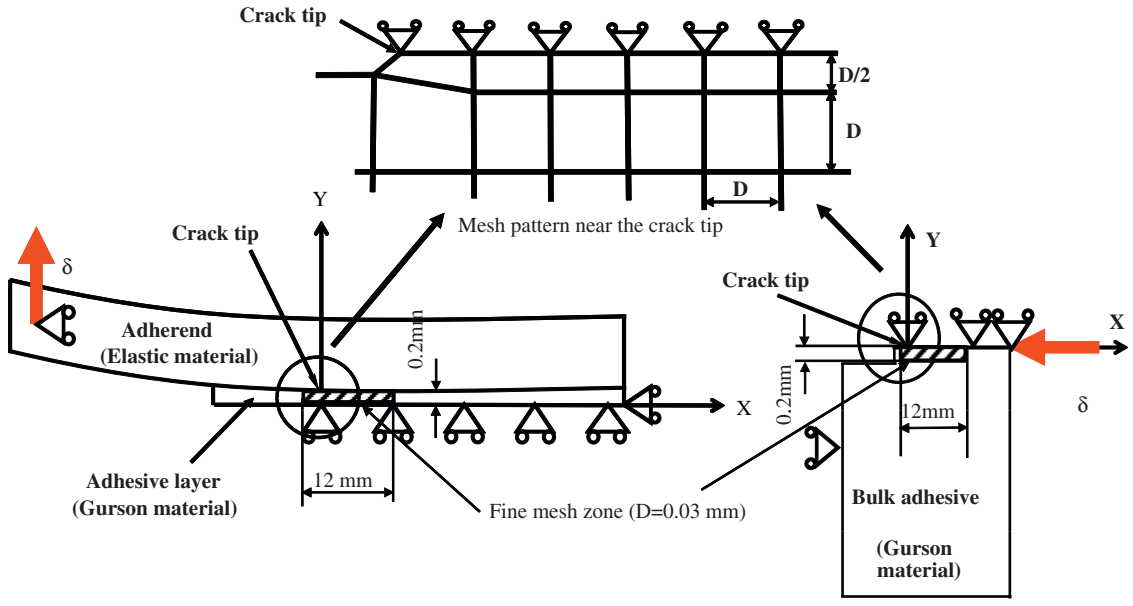

Fig. 10. Boundary conditions and coordinate system: (a) DCB specimen and (b) SENB specimen.

Hence, in this analysis, q_1 was tentatively determined to be 1.9, which was a value experimentally obtained from yield stresses of butt and scarf joints bonded by similar rubber-modified epoxy adhesive [22]. Based on the above assumptions, finite element calculations were made for six cases given in Table 3.

Fig. 11(a) and (b) shows the calculated load–displacement and crack extension-displacement curves for SENB and DCB specimens, respectively. For both specimens, the peak value of the curve increases with a decreasing initial void fraction. For the SENB specimen, the difference between the curves with and without nucleation is small, whereas, for the DCB specimen, nucleation leads to a broad peak. The figure also indicates NL points and crack initiation points where crack extension is nearly equal to 0.2 mm. Irrespective of the calculation conditions, crack initiation occurs just before reaching the peak points, and the difference between NL and crack initiation points for the DCB specimen is greater than that for the SENB specimen. Such a trend is similar to the experimental results in Fig. 4.

The discrepancy between the NL and crack initiation points is discussed in terms of the plastic distributions near the crack tip. Fig. 12 shows the contour of the plastic strain for DCB and SENB specimens just after crack initiation, in which Gurson's parameters correspond to case A in Table 3. The domain in which plastic strain is greater than 0.02 extends to 5.7 mm, forming the crack tip in the DCB specimen, whereas for the SENB specimen the domain is localized. Thus, it is expected that such a large damage zone in the DCB specimen would make the load–displacement curve deviate from linearity before crack initiation.

Fig. 13(a) and (b) shows the calculated R-curves for the SENB and DCB specimens together with the experimental data, wherein the ordinates are the J integral value and the energy release rate, respectively. The effects of the initial void fraction and nucleation on the behavior of the simulated R-curves for both SENB and DCB specimens were investigated. It was found that not only the values of J and G_{1C} but also the gradient of the R-curve increase with decreasing initial void fraction. In a previous study [23], several simulations for crack initiation and growth in tough metals have been conducted using Gurson's model, where the gradient of the R-curve also increases with decreasing initial void fraction. Thus, for both specimens, variation in the initial void fraction may be one cause of the difference

Table 3
Gurson's parameters used for FEM analysis

	q_1	q_2	Initial void traction, f_i	Void fraction at failure, f_E	Mean stress for void nucleation, σ_m (MPa)	Standard deviation, S (MPa)	Volume fraction of void forming particles, f_N	Object for simulation
A	1.9	1.0	0.14	0.6				CTBN-modified adhesive
B	1.9	1.0	0.01	0.3				DCS-modified adhesive
C	1.9	1.0	0.01	0.3	19.6	14.7	0.14	DCS-modified adhesive
D	1.9	1.0	0.01	0.3	19.6	9.8	0.14	DCS-modified adhesive
E	1.9	1.0	0.01	0.3	19.6	4.9	0.14	DCS-modified adhesive
F	1.9	1.0	0.01	0.3	19.6	1.96	0.14	DCS-modified adhesive

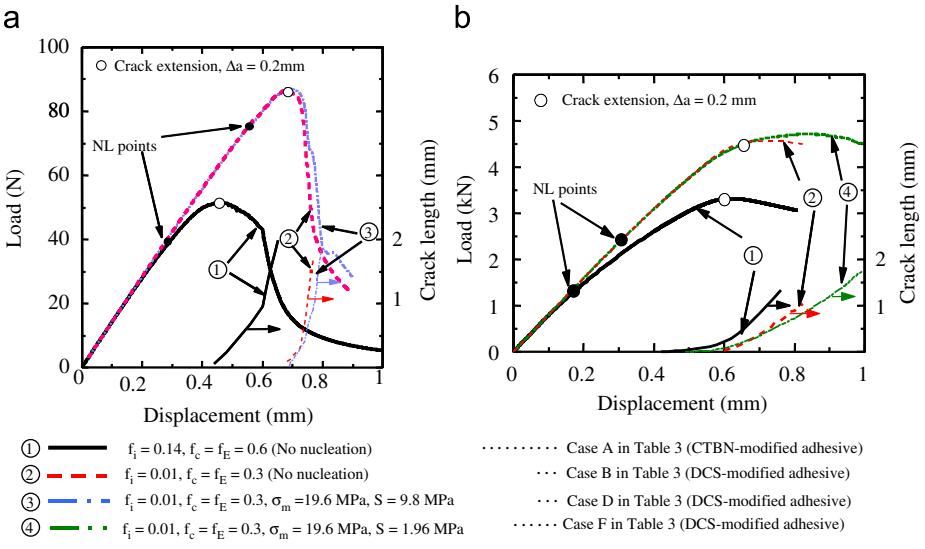

Fig. 11. Calculated load–displacement curves: (a) SENB specimens and (b) DCB specimens.

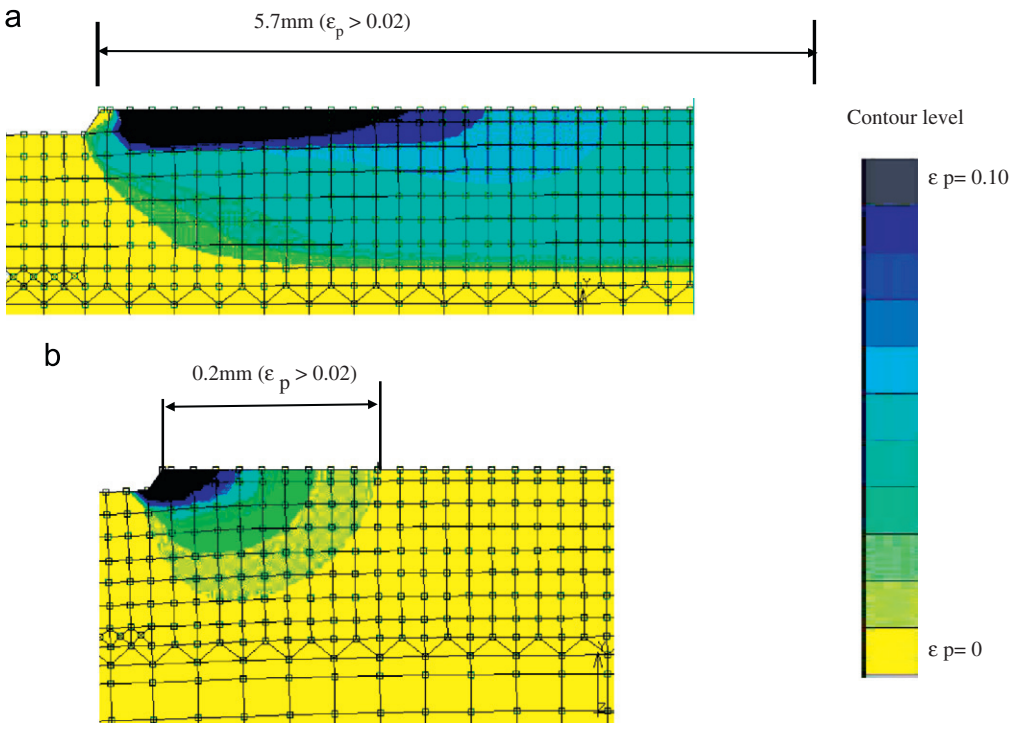

Fig. 12. Contour plots of plastic strain for (a) DCB specimen (case A in Table 3) and (b) SENB specimen (case A in Table 3) with CTBN-modified adhesive.

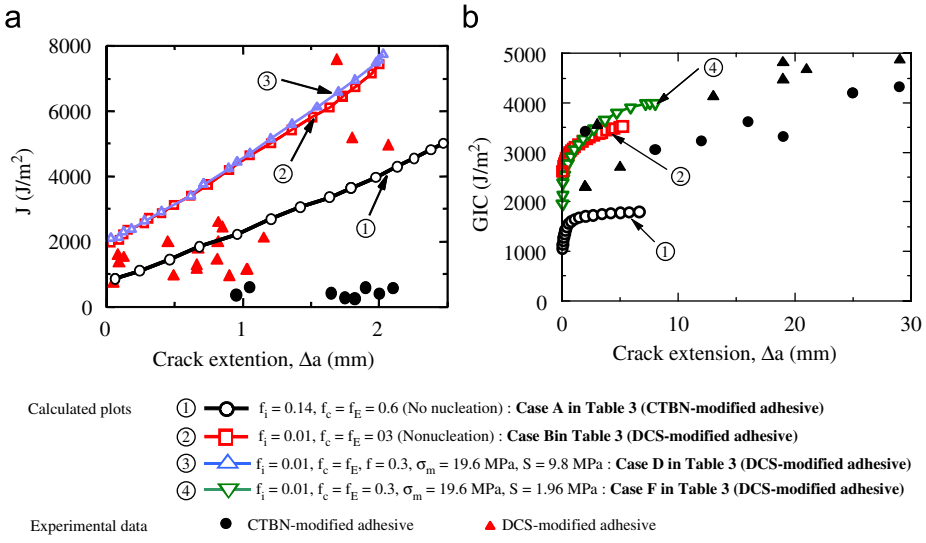

Fig. 13. Comparison between calculated and experimental *R*-curves: (a) SENB specimens and (b) DCB specimens.

in the slopes of *R*-curves between CTBN- and DCS-modified adhesives.

For the SENB specimen, the difference between the *J*–*R*-curves with and without nucleation is small as in Fig. 12, but the slope of the *R*-curve for the DCB specimen with nucleation is steeper than that without nucleation. This means that nucleation increases the slope of the *R*-curve of the DCB specimen; thus, nucleation is attributable to the difference in the slopes between DCS- and CTBN-modified adhesives.

To elucidate the effect of nucleation on the evolution of the damage zone, the contours of the void volume fraction near the crack tip are illustrated in Fig. 14 under the same crack extension with and without nucleation for the DCB specimen. The domain of the high void fraction extends to the inner area, irrespective of nucleation, and the area of the domain with nucleation is greater than that without nucleation. Such an extension of the damage zone may improve the capacity for absorbing fracture energy, which increases the energy release rate. Thus, we can conclude

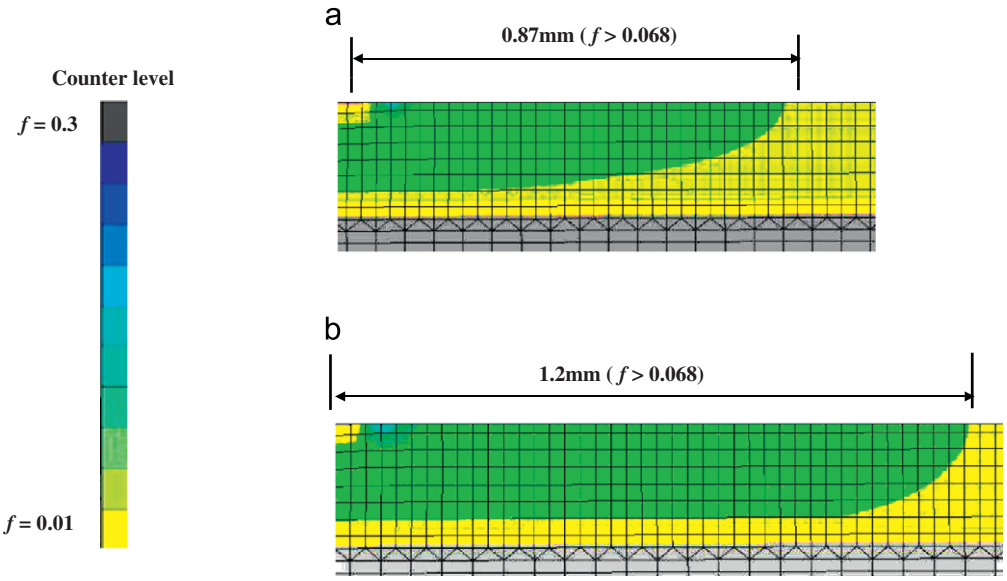

Fig. 14. Contour plots of the void volume fraction near the crack tip of DCB specimens ($\Delta a = 5.0$ mm): (a) $f_i = 0.01$, $f_F = 0.3$ (case B in Table 3) and (b) $f_i = 0.01$, $f_F = 0.3$, $S = 1.96$ MPa, $f_n = 0.14$ (case F in Table 3).

that nucleation causes the difference between the slopes mentioned above.

Comparing the calculated curves with the experimental plots in Fig. 13, the calculated values for DCS-modified adhesive are higher than the experimental values for both specimens. For the CTBN-modified adhesive, the calculated values of J for the SENB specimen are greater than the experimental values, whereas the calculated plots of G_{1C} for the DCB specimen are lower than the experimental results. Furthermore, the difference between calculated and experimental plots for CTBN-modified adhesive is greater than that for the DCS-modified one. As mentioned in the previous section, the damage zone formed not only ahead of the crack tip but also in the vicinity of the interface [16]. In the calculation, the damage zone in the vicinity of the interface was not taken into account. Thus, the calculated crack growth of the DCB specimens seems to be underestimated from the experimental data. This may be one reason for the discrepancy between calculated values and experimental data for CTBN-modified adhesive. Furthermore, for CTBN-modified adhesive, a part of liquid rubber dissolves in the epoxy phase. Thus, it is expected that the elastic–plastic properties of the matrix phase for CTBN-modified adhesive differ from those for the DCS-modified one which does not contain dissolved rubber.

5. Conclusions

R-curve characteristics of adhesively bonded DCB and bulk SENB specimens using rubber-modified epoxy resins were investigated, in which two different resin systems, i.e., liquid rubber (CTBN)- and cross-linked rubber particle (DCS)-toughened epoxies were used. Assuming that the resins are governed by Gurson's constitutive equation, the simulation of crack growth was conducted by FEM. The characteristics of the *R*-curves were discussed on comparison of the experimental observation with the simulation. Main results obtained in this work are as follows:

1. For SEBN specimens, the J-value of CTBN-modified adhesive is lower than that for the DCS-modified one, irrespective of crack extension. The slope of the J–Δa curve is very gentle for the CTBN-modified adhesive throughout the entire range of Δa. For DCS-modified adhesive, a gentle rise of J was observed with Δa smaller than 1 mm. Then, a sharp elevation in J occurred with further growth to about 2 mm. Hence, the intrinsic slope of the *R*-curve for DCS-modified adhesive is considered to be a little larger than that for CTBN-modified adhesive.
2. For DCB specimens, the value of G_{1C} for the DCB-modified adhesive shows a peak value at $\Delta a = 30$ mm and then slows down to a steady-state value of ~ 4 kJ/m^2. For the CTBN-modified adhesive, most data points for G_{1C} fall on a line with a smaller slope than the data for DCS-modified adhesive at $\Delta a < 20$ mm. Then, G_{1C} value gradually rose to a plateau value of ~ 4 kJ/m^2.
3. The fracture surface of SENB specimens shows that rubber particles are uniformly dispersed in CTBN-modified adhesive, whereas those in DCS-modified adhesive are localized. However, the matrix of DCS-modified adhesive was deformed more severely than that of the CTBN-modified one. For DCB specimens, the fracture surface of CTBN-modified adhesive was similar to that of SENB specimens. In contrast, for DCS-modified adhesive, the void fraction of the DCB specimen is lower than that of the SENB one, with its roughness being smaller than that of the SENB specimen.

4. The effect of the initial void fraction and nucleation on the behavior of the simulated *R*-curves was investigated for both SENB and DCB specimens. For these specimens, not only the values of J and G_{1C} but also the gradient of *R*-curves increased with decreasing initial void fraction. On the other hand, the effect of void nucleation on the characteristic of *R*-curve was small for the SENB specimens, whereas void nucleation increased the slope of *R*-curves for the DCB specimens. In conclusion, the decrease in the initial void fraction and nucleation could cause a difference in the slope of the *R*-curve between DCS- and CTBN-modified adhesives.

References

[1] Hunston DL, Kinloch AJ, Wang SS. Micromedianics of fracture in structural adhesive bonds. J Adhes 1989;28:103–14.

[2] Daghyni HR, Ye L, Mai Y-W. Mode I fracture behavior of adhesive joints, Part I. Relationship between fracture energy and bond thickness. J Adhes 1995;53:149–62.

[3] Rakestraw MD, Taylor MW, Dillard DA, Cheng T. Time dependent crack growth and loading effect on interfacial and cohesive fracture of adhesive joints. J Adhes 1995;55:123–49.

[4] Sue H-J, Meitin EIG, Pickelman DM, Bott CJ. Fracture mechanisms inrigid core–shell particle modified high performance epoxies. Colloid Polym Sci 1996;274:342–9.

[5] Qian JY, Person RA, Dimonie VL, Shaffer OL, EI-Aasser MS. The role of dispersed phase morphology on toughening on epoxies. Polymer 1997;38:21–30.

[6] Ormatxea M, Forcada J, Mugika F, Valea A, Martin MD, Marieta C, et al. Ultimate properties of rubber and core–shell modified epoxy matrices with different chain flexibilities. J Mater Sci 2001;36: 845–52.

[7] Fan L, Cantwell WJ, Kausch HH. The role of cavitation and debonding in the toughening of core–shell rubber modified epoxy systems. J Mater Sci 1997;32:3055–9.

[8] Yan C, Xiao K, Mai Y-W. Numerical and experimental studies on the fracture behavior of rubber-toughened epoxy in bulk specimen and laminated composites. J Mater Sci 2002;37:921–7.

[9] Imanaka M, Nakamura Y, Nishimura A, Iida T. Fracture toughness of rubber-modified epoxy adhesives: effect of plastic deformability of matrix phase. Comp Sci Tech 2003;63:41–51.

[10] Du J, Thouless MD, Yee AF. Development of a process zone in rubber-modified epoxy polymers. Int J Fract 1998;92:271–85.

[11] Blackman BPK, Hadavinia H, Kinloch AJ, Parasch M, Williams JG. The calculation of adhesive fracture energies in mode I: revisiting the tapered double cantilever beam (TDCB) test. Eng Fract Mech 2003;70:233–48.

[12] Blackman BPK, Parasch M, Kinloch AJ. The determination of the mode I adhesive fracture resistance, G_{1C}, of structural adhesive joints: an effective crack length approach. Eng Fract Mech 2005;72:897–977.

[13] ASTM Designation: E-1820-99a, standard test method for measurement of fracture toughness. In: Annual book of ASTM standard, section 3, vol. 03.01.2000.

[14] Cotterell B, Mai Y-W. Fracture mechanics of cementitious materials. London: Blackie Academic & Professional; 1996.

[15] Daghyani HR, Ye L, Mai Y-W. Effect of thermal residual stress on the crack path in adhesively bonded joints. J Mater Sci 1996;31: 2523–9.

[16] Lee D-B, Ikeda T, Miyazaki N, Choi N-S. J Mater Sci Lett 2003;22: 229–33.

[17] Gurson AL. Continumm theory of ductile rupture by void nucleation and growth, Part 1. Yield and flow rule for porous ductile media. J Eng Mater Tech 1977;99:2–15.

[18] Tvergaard V. Influence of void nucleation on ductile shear fracture at free surface. J Mech Phys Solids 1982;30:399–425.

[19] Lazzeri A, Bucknall CB. Recent developments in the modeling of dilational yielding in toughened plastics. In: Person RA, Sue H-J, Tee AF, editors. Symposium series #759 on toughening of plastics, American Chemical Society, Washington, DC; 2000. p. 86–96.

[20] Ikeda T, Mano J, Ikemoto D, Lee DB, Miyazaki N. Constraint effect of the fracture of adhesive joint (2nd Report, Failure analysis around a crack tip using Gurson's model). Trans Jpn Soc Mech Eng 2003; 69:210–7 (in Japanese).

[21] Tverrgard V. On localization in ductile materials containing spherical voids. Int J Fract 1982;18:237–52.

[22] Imanaka M, Suzuki Y. Yield behavior of rubber-modified epoxy adhesives under multiaxial stress condition. J Adhes Sci Technol 2002;11:1687–700.

[23] Xia L, Shih CF, Hutchinson JH. A computational approach to ductile crack growth under large scale yielding conditions. J Mech Solids 1995;43:389–413.